Dynamic modeling of defective gears

Alin-Virgil Bloju, Zoltan-Iosif Korka*

Abstract*. The use of geared transmissions has a long history and a rich experience, which has allowed the development of an intense research activity that has led to modern design methods, mostly standardized and execution technologies that have become traditional. As the fundamental sciences have provided more and more in-depth and refined knowledge, namely performance algorithms of optimal synthesis, the design in the field of gear transmissions has evolved by integrating in the calculation methods a growing number of elements. of influence (materials, geometry, dimensional and shape deviations, heat treatments, kinematic, energetic, dynamic factors, etc.). Automated modeling and simulation currently allow the prediction of behavior - from all points of view of a transmission - during operation.*

Keywords*: transmissions, modeling, simulation, calculation methods*

1. Introduction

Due to high service load, harsh operating conditions or fatigue, there may be a cause for a number of different drive-pattern [1]. Drive failures are responsible for approximately 60% of speed damage [2]. Most of these defects occur in the form of cracks, exfoliations or chipping [2]. According to Syncrude Canada Ltd, fatigue crack and tooth tongs, known as pitting, were the most common defects[3]. Cracks are a non-lubrication fault mode while pinching is a type of lubrication-related fault [2]. Many researchers have shaped the cracks in the gear and their effect on the stiffness of the teeth [4]. However, research on python modeling and its effect on the stiffness of the year-grenadier is limited. This reference focuses on the fault modeling in the form of pinching and investigating its effect on the thimple gear rigidity a pair of gears with external teeth.

According to the American society for metals (ASM) manual [5], pinch occurs when fatigue cracks are established on the surface of the tooth or just below the surface of the tooth. The chipping is usually surface cracks caused by metal-metal contact of sparsness, or occurs due to the low thickness of the lubricant film. On high-speed gears, with smooth surfaces and good oil film thickness, splits can occur due to cracks that start under the surface of the teeth side faces. These cracks may be

induced by the inclusion in the gear material, which acts as tension concentrators and propagates below and parallel to the tooth surface. The pinches form when the cracks cross the tooth surface and cause the material to separate. When several pits join, a larger pit (or an exfoliation) forms. Pinching can also occur due to contamination of the lubricant with foreign particles. These particles create points of tension in the oil film, reducing its load and thus promoting the initiation of the pitting.

Tan et al [6] have experimentally measured the growth of the pectates at different loading levels. In order to ensure the bearing of the lubricating film, SAE 20W-50 type oil has been used within a relatively short time. But it has poor wear properties. The experimental tests were carried out at a rotational speed of 745 rpm at different torque moments: 220Nm, 147Nm and 73Nm.

For the conditions with higher applied torque moments (220Nm and 147Nm), the pitching was manifested over the full width of the teeth and was visible on most of the gear teeth. For the lower torque applied (73 Nm), the pitching spread over the width of the gear teeth at a much slower speed and was located only a few teeth. Prolonged operating time has spread splashes on the gear teeth. Figure 1 shows the time progression of the affected area from 6,3% to 41,7% of the gear tooth surface under the test conditions at 73 N m and 745 rpm.
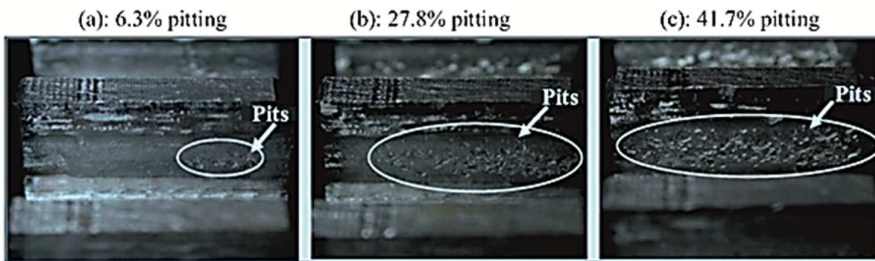
Figure 1. Pinch rise under 73 N m and 745 rpm operating conditions [6].

Hand-produced ruffles, to simulate the tetching, were practiced on the teeth of the gear by several researchers to explore experimentally the symptoms corresponding to the defect of a box. Gelman et al [2] made tooth surface depths by artificial etching along the tilt line of a single tooth to imitate the pitching. Lee and colab. [7] created a pinch on the top dusty tooth, removing by processing a small part of the tooth material. Combet et al [5] manually produced pinches on the side of five teeth. The chipped teeth were not successive, but separated by six flawed teeth. Öztürk et al [8] they first created circular pinches on a tooth using an electro-erosion machine. Then they added several such recesses of the same size to the same tooth. Also, they were created on the deep neighboring teeth to materialize the initiation of the

pitting fault. Hoseini et al [3] artificially created circular chipping on a planetary gear, using electrical erosion processing. The number of pinches was varied to mimic slight, moderate and severe damage, as shown in Figure 2. In this study, we have also shaped the drive teeth pinching using circular holes, as was done in [3,8].

| a. | b. | c. |
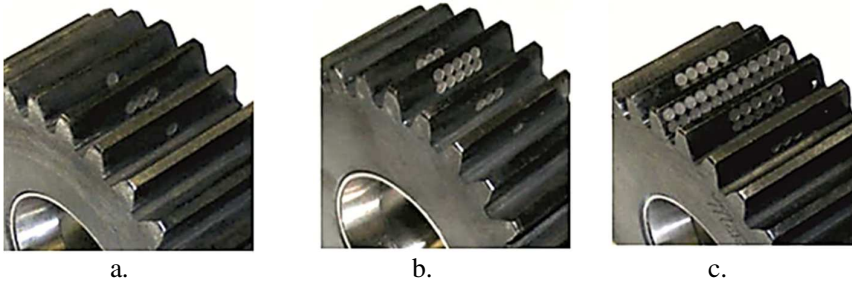
Figure 2. Gears with a Pitting gear created by artificial cipas [3]
(a-pitting light, b-moderate; c-severe pitting)

Several researchers have investigated the effect of a single pinch or exfoliation on the limable stiffness of the gear over time. Chaar et al [9] and Choy et al respectively. [10] changed the form of variation of the rigidity of the gear to simulate the assembly defect. They did not provide any principle or equation to determine the rigidity of the gear as the pup-re defect increased. Cheng et al [16], Aboul-Seoud et al [12] respectively Chaar et al [1] analyzed the effect of a single stump on the variable stiffness in time of the gear. The pinypid was shaped as a rectangular shape, as shown in Figure 3. In Cheng's model, the length of the pinch a and the width of the pinch b were fixed, while the severity of the pups was determined by the depth of the pinching c. In the model of Aboul-Seoud, the pinched width b and the size of the pebure were fixed, while the severity of the pinch was determined by its length a.
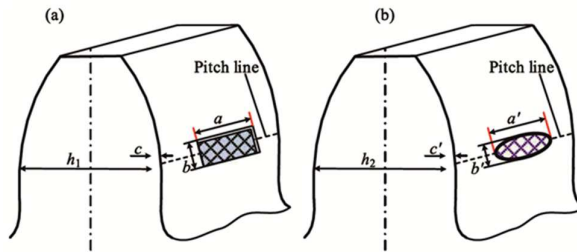
Figure 3. Chipping patterns for assessment of rigidity of gear networks.(a);(b)

Chaar et al [1] developed two models in their study. One is the same as Cheng's model [11], while the other is the same as the model of Aboul-Seoud [12]. RAC et al [13] evaluated the effect of cipire/pyttering on the variation in time of the stiffness of a gear using the final element method. Only one pinch was shaped in elliptical form, as shown in Figure 3 (b). The size of the pinch was fixed, but the effect of the defect position on the rigidity of the gear was investigated. Three pinched positions were examined, namely the unipolar gear area (when a pair of teeth engages), the bipolar contact area (when two pair of teeth are in simultaneous mesh) and the transition area from unipolar to bipolar gear. MA and colab [14] have investigated the effect of tooth cidation on the rigidity of the gear. A unique rectangular exfoliation has been modeled and investigated the effects of width, length and exfoliation site on rigidity. All the above studies to assess the rigidity of the gear pair shall focus on the existence of a single pinch. Their methods cannot be used to assess the rigidity of the drive on wheels with several pits on one tooth. Yang and Lin's study [15] addressed this shortcoming. Later, Tian and colab [16] added the shear-care energy to the potential energy method. The potential energy method has been used to assess the rigidity of gears without defects [14,15], on gears with cracks [4,11,16], on single chipped gears on one tooth [12], on gears with a chipped tooth [16], on gears with a change in the tooth profile [14], plastic tooth-deflection gears [14] and alignment-fault gears (mounting) [18]. The energy method was used in this study to assess the stiffness of the anaging of a pair of external gears with several shells on one tooth.

In this research, the tooth-pinch was shaped as circular. The equations to test the rigidity of the drive with several pinches on one tooth have been inferred using the method of potential energy. A case study was then presented to illustrate the effect of pitting on the rigidity of an agrenal. Three levels of pitching severity have been modeled: Light, moderate and severe. Finally, the proposed method was compared to a model using the finished element to verify its accuracy.

2. Calculation of the stiffness of gears with Pitting

For this purpose, the stumps have been shaped in circular form, as in [3,8]. The potential energy method [15,17] was used to write the rigidity equations for the gear pair. In [15, 17] angre-naing is assumed to be free of friction, no manufacturing errors and no transmission error. The gear body is treated as rigid. The rigidity of the drive has been calculated according the rotation angle of the drive. In the first stage, the rigidity equations of the gear were obtained with a single weird tooth. These equations were then extended to gears with more pinches per tooth.

71

2.1. Calculation of the stiffness of gears with a single shank on the tooth

For assessment of the rigidity of the drive without fault, in [17] the tooth was modeled as a beam in the bracket as shown in Figure 4(a).
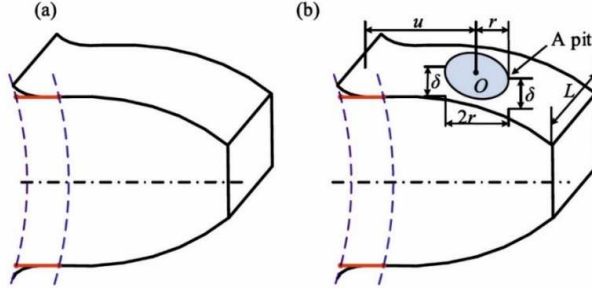
Figure 4. Tooth modeling: (a) a tooth model for gears without damage and (b) the proposed single shank tooth model.

In the first stage, only one circular chip was considered as shown in Figure 4. The acre delimits the pinch is located on the side of the tooth. The position and size of a single shank can be fully characterized by three variables: *(u, r, δ)*, where *u* represents the distance between the tooth leg and the center of the circle of the peeling, *r* is the radius of the chip and *δ* is the depth of the chip. The position of the chip in the direction *δ* of the tooth (the width of the tooth is as shown in Figure 4.b) is not unrred in the proposed method.

2.2 Curvy, shear and axial compressiveness

Depending on the properties of the volute curve, the action line of the two networks is tangent to the base circles of the gear and normal to the volute profile of the tooth. The action force F which is along the action line may be broken down into two orogonal forces F_a and F_b, as shown in Figure 5.

$$F_a = F \sin \alpha_1 \tag{1}$$
$$F_b = F \cos \alpha_1 \tag{2}$$

Applying the potential energy method, the bending, shear and axial compression energies stored in a tooth can be expressed as follows [15]:

$$U_b = \frac{F^2}{2k_b} = \int_0^d \frac{[F_b(d-x) - F_a h]^2}{2EI_x} dx, \tag{3}$$
$$U_s = \frac{F^2}{2k_s} = \int_0^d \frac{1.2F_b^2}{2GA_x} dx, \tag{4}$$

$$U_a = \frac{F^2}{2k_a} = \int_0^d \frac{F_a^2}{2EA_x}\,dx, \tag{5}$$
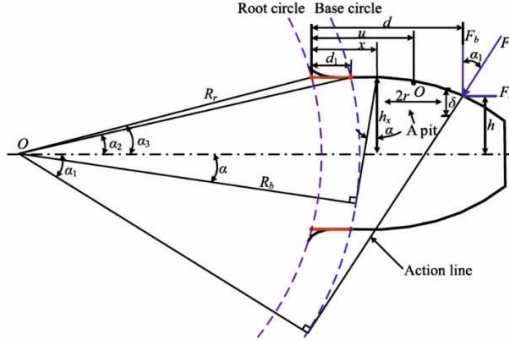
Figure 5. Spring force on a single-shank gear tooth.

Where k_b, k_s and k_a represent the stiffness to bend, shear and axial compression respectively, E and G repretighten the young module and the shear module respectively, i.e. the distance between the point of contact of the gear and the center line of the tooth, d is the distance between the point of contact of the gear and the gear train's backside, A and I_x indicate the area and time of the inertia area of the tooth section, i.e. the distance from the root of the tooth x.

Depending on the characteristics of the curve, h, h_x, d, x, A_x and I_x of a perfect gear tooth can be expressed as follows [17]:

$$h = R_b[(\alpha_1 + \alpha_2)\cos\alpha_1 - \sin\alpha_1], \tag{6}$$

$$h_x = \begin{cases} R_b\sin\alpha_2, & \text{if } d_1 < x \le d_1 \\ R_b[(\alpha + \alpha_2)\cos\alpha - \sin\alpha], & \text{if } d_1 < x \le d' \end{cases} \tag{7}$$

$$d = R_b[(\alpha_1 + \alpha_2)\sin\alpha_1 + \cos\alpha_1] - R_r\cos\alpha_3, \tag{8}$$

$$x = R_b[(\alpha + \alpha_2)\sin\alpha + \cos\alpha] - R_r\cos a_3, \tag{9}$$

$$A_x = 2h_x L, \tag{10}$$

$$I_x = \frac{1}{12}(2h_x)^3 L = \frac{2}{3}h_x^3 L, \tag{11}$$

Where R_b, R_l and L represent the radius of the base circle, the radius of the root circle and the tooth width of the outer wheel, h, signifies the height of the section whose distance to the tooth root is x, α_2 is the angle of rotation of the teeth on the

73

base circle, α_3 describes the approximate angle of half of the root circle and α is the angle of rotation of the gear (see Fig.5). Angle expressions are given as follows [17].

$$\alpha_2 = \frac{\pi}{2Z} + \tan \alpha_0 - \alpha_0, \tag{12}$$

$$\alpha_3 = arcsin\left(\frac{R_b \sin \alpha_2}{R_r}\right), \tag{13}$$

Where Z is the number of teeth of the outer wheel and α_0 is the pressure angle.

For a hollow tooth gear, the expressions h, h_x, I_x şi A_x are different from those given above for a perfect gear tooth. In addition, the contact width of the teeth is not constant L. We use ΔL_x şi ΔA_x şi ΔI_x to represent the reduction in the width of the teeth contact, the zone and the moment of the inertia zone of the teeth section, i.e. the distance to contact with the gear. For a single pipet model on a tooth, in Figure 4.b, the expression ΔL_x şi ΔA_x şi ΔI_x is as follows:

$$\Delta L_x = \begin{cases} 2\sqrt{r^2 - (u-x)^2}, & x \in [u-r, \ u+r] \\ 0, & others \end{cases} \tag{14}$$

$$\Delta A_x = \begin{cases} \Delta L_x \delta, & x \in [u-r, \ u+r] \\ 0, & others \end{cases} \tag{15}$$

$$\Delta I_x = \begin{cases} \frac{1}{12}\Delta L_x \delta^3 + \frac{A_x \Delta A_x (h_x - \delta/2)^2}{A_x - \Delta A_x}, & x \in [u-r, \ u+r] \\ 0, & \end{cases} \tag{16}$$
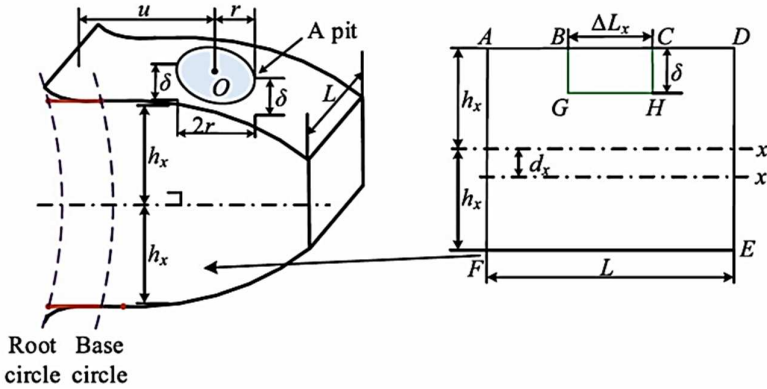
Figure 6. A section of a single shank tooth.

Figure 6 shows a section of the tooth of a gear with a single shank. Let's use I_x şi I_{x2} to represent the moments of inertia of the a-B-C-D-E-F and A-B-G-H-C-D-E-F tooth sections in relation to the x-axis respectively. Use I_x to represent the moment of inertia of the area in section A-B-G-H-C-D-E-F about the x' axis, where x' is the

center-center axis of the a-B-G-H-C-D-E-F. Folo-sind the theory of the parallel axis [15, 19], we can achieve:

$$I_x = I_{x2} + \frac{1}{12}\Delta L_x \delta^3 + \Delta L_x \delta \left(h_x - \frac{\delta}{2}\right)^2, \tag{17}$$

$$I_{x2} = I_{x'} + (2h_x L - \Delta L_x \delta)(d_x)^2, \tag{18}$$

By combining equations (17) and (18) we can obtain:

$$I_{x'} = I_x - \frac{1}{12}\Delta L_x \delta^3 - \frac{A_x \Delta A_x (h_x - \delta/2)^2}{A_x - \Delta A_x}, \tag{19}$$

Use $\Delta I_x = I_x - I_{x'}$ to represent the reduction in the zones of inertia in the section of the tooth. We can obtain the equation (16).

Given a gear tooth with a circular hollow, we can calculate ΔL_x și ΔA_x and ΔI_x for any section of the teeth whose distance to the point of contact with the gear is x. In addition, pu-TEM notes from EC. (5) ca x is a function of the angle of rotation of speed (noted with the $\acute{\alpha}$). Therefore, for any given angle of rotation, we can calculate the values ΔL_x and ΔA_x and ΔI_x using EC. (14), (15) and (16) respectively. In addition, ΔL_x and ΔA_x and ΔI_x are all independant of the position of the chip in the direction of the width of the tooth. Therefore, the position of the chip along the width of the tooth is not required in these equations.

Replacement of equation (1), (2), (6) to (9), (14) to (16) in (3), the bending rigidity of an external gear tooth with a circular toothpick can be obtained:

$$\frac{1}{k_b} = \frac{\left[1 - \frac{(Z - 2,5)\cos \alpha_1 \cos \alpha_3}{N \cos \alpha_0}\right]^3 - (1 - \cos \alpha_1 \cos \alpha_2)^3}{2EL \cos \alpha_1 \sin^3 \alpha_2}$$
$$+ \int_{-\alpha_1}^{\alpha_2} \frac{3\{1 + \cos \alpha_1 [(\alpha_2 - \alpha)\sin \alpha - \cos \alpha]\}^2 \ (\alpha_2 - \alpha)\cos \alpha}{E\left(2L[\sin \alpha + (\alpha_2 - \alpha)\cos \alpha]^3 - 3\frac{\Delta I x}{R_b^3}\right)} d\alpha. \tag{20}$$

Replacing equations (1), (7) to (10), (14) to (15) in equation (5), the axial compressive stiffness of an external gear tooth can be obtained with a circular toothpick:

$$\frac{1}{k_s} = \frac{1.2(1 + v)cos^2 \ \alpha_1 \left(\cos \alpha_2 - \frac{Z - 2.5}{Z \cos \alpha_0}\cos \alpha_3\right)}{EL \sin \alpha_2} +$$
$$\int_{-\alpha_1}^{\alpha_2} \frac{1.2(1 + v)(\alpha_2 - \alpha)\cos \alpha \cos^2 \alpha_1}{E\left(L[\sin \alpha + (\alpha_2 - \alpha)\cos \alpha] - \frac{\Delta A x}{2R_b}\right)} \ d\alpha. \tag{21}$$

Replacing equations (1), (7) to (10), (14) to (15) in equation (5), the axial compressive stiffness of an external gear tooth can be obtained with a circular toothpick:

$$\frac{1}{k_a} = \frac{sin^2\,\alpha_1\left(\cos\alpha_2 - \frac{Z-2.5}{Z\cos\alpha_0}\cos\alpha_3\right)}{2EL\sin\alpha_2} + \int_{-\alpha_1}^{\alpha_2} \frac{(\alpha_2-\alpha)\cos\alpha\,sin^2\,\alpha_1}{E\left(2L[\sin\alpha+(\alpha_2\,\alpha)\cos\alpha] - \frac{\Delta A_x}{R_b}\right)}\,d\alpha. \quad (22)$$

Expression $\acute\alpha 1$, is given [18]:

$$\alpha_1 = \theta - \frac{\pi}{2Z_1} - \tan\alpha_0 + \alpha_0 +$$

$$tan\left[arccos\frac{Z_1\cos\alpha_0}{\sqrt{(Z_2+2)^2+(Z_2+Z_1)^2-2(Z_2+2)(Z_2+Z_1)cos\left(arccos\frac{Z_2\cos\alpha_0}{Z_2+2}-\alpha_0\right)}}\right] \quad (23)$$

Where Z_1 și Z_2 represent the number of teeth in the box, and respect θ is the gearbox's SI rotation angle and we can define $\theta = 0$ when the pinched tooth starts to mesh.

With regard to the pair tooth of the rib tooth, equations (20) to (22) can still be used to calculate the rigidity of its network as long as it is an external gear tooth. However, the expression of α_1 is expressed as [16]:

$$\alpha_1 = tan\left(arccos\frac{Z_2-\cos\alpha_0}{Z_2+2}\right) - \frac{\pi}{2Z_2} - \tan\alpha_0 + \alpha_0 - \frac{Z_1}{Z_2}\theta. \quad (24)$$

2.3. Hertzian contact stiffness

From the results obtained by Yang and Sun [11], the radio contact stiffness, for a pair of perfect external wheels, is linearized to a constant throughout the whole line of action, irrespective of both the contact position and the depth of the interpenetration.

$$k_h = \frac{\pi EL}{4(1-\nu^2)'} \quad (25)$$

Where E, L, υ, the boardweight denotes the mode of Young, and the width of the tooth and the Poisson report respectively.

For a pair of toothed wheels, the contact width of the tooth is L-ΔL_x and not L. If the torque meter is used for the measurement of the torque meter, the torque meter shall be set to a minimum of 5 % of the input torque.

$$k_h = \frac{\pi E(L-\Delta L_x)}{4(1-\nu^2)}, \quad (26)$$

Where Ddlx, is the reduction in the width of contact between the teeth (see equation (14).

2.4. Difference in stiffness of the gear train with several tooth pitting

In section 1, we derived the rigidity equations of the drive network with a single stump. These equations can be easily extended to gears with several circular splashes on one tooth. As long as the circular splits do not overlap with each other

and all the circles are within the area of the tooth surface, the hertzian contact strength, bending rigidity, shear stiffness and axa-to-a compressive stiffness can be obtained by equations (27), (28), (29) and (30) respectively:

$$k_h = \frac{\pi E\left(L - \sum_1^N \Delta L_{xj}\right)}{4(1-v^2)}, \tag{27}$$

$$\frac{1}{k_b} = \frac{\left[1 - \frac{(Z-2.5)\cos\alpha_1\,\cos\alpha_3}{Z\cos\alpha_0}\right]^3 - (1-\cos\alpha_1\,\cos\alpha_2)^3}{2EL\,\cos\alpha_1\,sin^3\,\alpha_2}$$
$$+ \int_{-\alpha_1}^{\alpha_2} \frac{3\{1+\cos\alpha_1[(\alpha_2-\alpha)\sin\alpha-\cos\alpha]\}^3\,(\alpha_2-\alpha)\cos\alpha}{E(2L\,[\sin\alpha+(\alpha_2-\alpha)\cos\alpha]^3)-3\sum_1^N\frac{\Delta I_{xj}}{R_b^3}}\,d\alpha, \tag{28}$$

$$\frac{1}{k_s} = \frac{1.2(1+v)cos^2\alpha_1\left(\cos\alpha_2 - \frac{Z-2.5}{Z\cos\alpha_0}\cos\alpha_3\right)}{EL\sin\alpha_2}$$
$$+ \int_{-\alpha_1}^{\alpha_2} \frac{1.2(1+v)(\alpha_2-\alpha)\cos\alpha\,cos^2\alpha_1}{E\left(L[\sin\alpha+(\alpha_2-\alpha)\cos\alpha]-0.5\sum_1^N\frac{\Delta A_{xj}}{R_b}\right)}\,d\alpha, \tag{29}$$

$$\frac{1}{k_a} = \frac{sin^2\alpha_1\left(\cos\alpha_2-\frac{Z-2.5}{Z\cos\alpha_0}\cos\alpha_3\right)}{2EL\sin\alpha_2} + \int_{-\alpha_1}^{\alpha_2} \frac{\left(\alpha_2-\frac{Z-2.5}{Z\cos\alpha_0}\cos\alpha_3\right)}{E\left(2L[\sin\alpha+(\alpha_2-\alpha)\cos\alpha]-\sum_1^N\frac{\Delta A_{xj}}{R_b}\right)}\,d\alpha, \tag{30}$$

Where N is the number of circular toothcuts on a tooth surface; ΔL_{xj}, ΔA_{xj} and ΔI_{xj} is the reduction of the tooth contact width, area and moment zone of inertia caused by the circular sheet, ΔL_{xj}, ΔA_{xj} and ΔI_{xj} can be obtained using equations (14), (15) and (16) respectively.

Users may apply these equations to assess the rigidity of the gear train at any given ro-speed angle, even if they are not familiar with the theory of these networks.

3. Conclusions

Fault feature analysis of gear tooth spall plays a vital role in gear fault diagnosis. Knowing the characteristic of fault features and their evolution as a gear tooth fault progresses is key to fault severity assessment. This thesis provides a comprehensive (both theoretical and experimental) analysis of the fault vibration features of a gear transmission with progressive localized gear tooth pitting and spalling. A dynamic model of a one-stage spur gear transmission is proposed to analyze the vibration behavior of a gear transmission with tooth fault. The proposed dynamic model considers the effects of Time Varying Mesh Stiffness (TVMS), tooth surface roughness changes and geometric deviations due to pitting and spalling, and also incorporates a time-varying load sharing ratio, as well as dynamic tooth contact friction forces, friction moments and dynamic mesh damping ratios. The gear dynamical model is validated by comparison with responses obtained from an

experimental test rig under different load and fault conditions. In addition, several methods are proposed for the evaluation of the TVMS of a gear pair with tooth spall(s) with curved bottom and irregular shapes, which fills the current research gap on modelling tooth spalls with irregular shapes and randomly distribution conditions. Experiments are conducted and the fault vibration features and their evolution as the tooth fault progresses are analyzed. Based on feature analysis, a new health indicator is proposed to detect progressive localized tooth spall.

References

[1] Chaari F., Baccar W., Ab bes M.S., Haddar M., Effect of spalling or tooth breakage on gearmesh stiffness and dynamic response of a one-stage spur gear transmission, *Eur.J. Mech. A Solids,* 27(4), 2008, pp. 691-705.

[2] Gelman L., Zimroz R., Birkel J., Leigh-Firbank H., Simms D., Waterland B., Whitehurst G., Adaptive vibration condition monitoring technology for local tooth damage in gearboxes, *Insight Non-Destr. Test. Cond. Monit.* 47(8), 2005, pp. 461-464.

[3] Hoseini M.R., Zuo M.J., *Literature review for creating and quantifying faults in planetary gearboxes*, Technical Report, Reliability Research Lab, Mechanical Department, University of Alberta, 2009.

[4] Ma H., Zeng J., Feng R., Pang X., Wang Q., Wen B., Review on dynamics of cracked gear systems, *Eng. Fail. Anal.* 55, 2015, pp. 224-245.

[5] Blau P.J., *ASM Handbook, Vol. 18 - Friction, lubrication, and wear technology*, ASM International, 1992.

[6] Tan C.K., Irving P., Mba D., A comparative experimental study on the diagnostic and prognostic capabilities of acoustics emission, vibration and spectrometric oil analysis for spur gears, *Mech. Syst Signal Process*. 21(1), 2007, pp. 208-233.

[7] Ozti.irk H., Sabuncu M., Yesilyurt I., Early detection of pitting damage in gears using mean frequency of scalogram, *J. Vib. Control* 14(4), 2008, pp. 469-484.

[8] Choy F.K., Polyshchuk V., Zakrajsek J.J., Handschuh R.F., Townsend D.P., Analysis of the effects of surface pitting and wear on the vibration of a gear transmission system, *Tribol. Int.* 29(1), Feb. 1996, pp. 77-83.

[9] Abouel-seoud S.A., Dyab E.S., Elmorsy M.S., Influence of tooth pitting and cracking on gear meshing stiffness and dynamic response of wind turbine gearbox, *Int. J. Sci. Adv. Technol*. 2(3), 2012, pp. 151-165.

[10] del Rincon A.F., Viadero F., Iglesias M., de-Juan A., Garcia P., Sancibrian R., *Effect of cracks and pitting defects on gear meshing*, Proc. Inst. Mech. Eng. Part CJ. Mech. Eng. Sci. 226(11), 2012, pp. 2805-2815.

[11] Ma H., Li Z., Feng M., Feng R., Wen B., Time-varying mesh stiffness calculation of spur gears with spalling defect, *Eng. Fail. Anal*. 66, 2016, pp. 166-176.

[12] Yang D.C.H., Lin J.Y., Hertzian damping, tooth friction and bending elasticity in gear impact dynamics, *J. Mech. Des*. 109(2), 1987, pp. 189-196.

[13] Tian X., Zuo M.J., Fyfe K.R., *Analysis of the vibration response of a gearbox with gear tooth faults*, In: Proceedings of the Presented at the 2004 ASME International Mechanical Engineering Congress and Exposition, Anaheim, California USA, 2004, pp. 785-793.

[14] Liang X., Zuo M.J., Patel T.H., *Evaluating the time-varying mesh stiffness of a planetary gear set using the potential energy method*, Proc. Inst. Mech. Eng. Part CJ. Mech. Eng. Sci. 228(3), 2014, pp. 535-547.

[15] Chen Z., Shao Y., Dynamic simulation of spur gear with tooth root crack propagating along tooth width and crack depth, *Eng. Fail. Anal*., 18(8), 2011, pp. 2149-2164.

[16] Pandya Y., Parey A., Failure path based modified gear mesh stiffness for spur gear pair with tooth root crack, *Eng. Fail. Anal*. 27, 2013, pp. 286-296.

[17] Chen Z., Shao Y., Mesh stiffness calculation of a spur gear pair with tooth profile modification and tooth root crack, *Mech. Mach. Theory*, 62, 2013, pp. 63-74.

[18] Cao Z., Shao Y., Zuo M.J., Liang X., *Dynamic and quasi-static modeling of planetary gear set considering carrier misalignment error and varying line of action along tooth width*, Proc. Inst. Mech. Eng. Part CJ. Mech. Eng. Sci. 229(8), 2015, pp. 1348-1360.

[19] Sainsot P., Velex P., Duverger O., Contribution of gear body to tooth deflections - a new bidimensional analytical formula, *J. Mech. Des.* 126(4), 2004, 748.

Addresses:

- Drd.Eng. Alin-Virgil Bloju, Babeș-Bolyai University, Faculty of Engineering, Piaţa Traian Vuia, nr. 1-4, 320085, Reşiţa, alin.bloju@ubbcluj.ro
- Assoc. Prof. dr. eng. habil. Zoltan-Iosif Korka, Babeș-Bolyai University, Faculty of Engineering, Piaţa Traian Vuia, nr. 1-4, 320085, Reşiţa, zoltan.korka@ubbcluj.ro
([*] corresponding author)